PAPER

Check for updates

Customized CO_2 electroreduction to methane or ethylene by manipulating *H and *CO adsorption on Cu/CeO$_x$ catalysts†

Tinghui Yang, Yingbing Zhang, Zichao Huang, Jianping Yang [ID] * and Min Kuang [ID] *

The coverage of *CO and *H intermediates on the surface of a catalyst plays a pivotal role in determining the selectivity towards C_1 or C_2 products in the electrochemical CO_2 reduction reaction (CO$_2$RR). In this study, we engineered two types of interfaces involving copper and rare earth metal oxides, specifically Cu/CeO$_x$ and Cu/CuCeO$_x$ solid solution, which exhibit enhanced binding affinities for *H and *CO adsorbates in the CO$_2$RR, respectively. As a result, the Cu/CuCeO$_x$ catalyst delivered an ethylene faradaic efficiency of 40.2% at a partial current density of -245.7 mA cm^{-2}, whereas the Cu/CeO$_x$ catalyst presented a methane faradaic efficiency of 38.6% at a partial current density of -198.3 mA cm^{-2}. Results of theoretical and experimental analyses have demonstrated that the Cu–Ce–O$_x$ solid solution markedly enhances *CO adsorption by stabilizing Cu$^+$ species, thereby favoring its dimerization to ethylene rather than converting to methane through hydrogenation. This investigation elucidates a strategy for directing the selective electroproduction of C_1 or C_2 compounds from the CO$_2$RR by effectively manipulating *H and *CO adsorption on Cu/CeO$_x$ catalysts.

Introduction

The relentless rise in atmospheric CO_2 levels, predominantly driven by anthropogenic activities, has been identified as a principal factor exacerbating global warming, eliciting widespread concern across the globe.[1,2] Within this critical context,

State Key Laboratory for Modification of Chemical Fibers and Polymer Materials, College of Materials Science and Engineering, Donghua University, Shanghai 201620, China. E-mail: jianpingyang@dhu.edu.cn; mkuang@dhu.edu.cn

† Electronic supplementary information (ESI) available. See DOI: https://doi.org/10.1039/d4ta01808g

Min Kuang is currently a professor in the College of Materials Science and Engineering at Donghua University, China. She received her PhD from the Laboratory of Advanced Materials at Fudan University. Following this, she joined the School of Materials Science and Engineering at Nanyang Technological University as a postdoctoral research associate. Her research focuses on developing advanced electrochemical C_1-to-fuel conversion systems and exploring efficient electrocatalysts.

Min Kuang

the electrochemical carbon dioxide reduction (CO$_2$RR), especially when powered by renewable energy sources like solar and wind, has emerged as a vital strategy for carbon balance restoration.[3–5] Distinct from the generation of simpler C_1 products like formic acid (HCOOH) and carbon monoxide (CO),[6] there is an intensified demand for the production of high energy density hydrocarbons, notably methane (CH$_4$) and ethylene (C$_2$H$_4$), which are envisioned as potential sustainable fuels.[7–9] To date, copper-based materials, endowed with optimal adsorption energy for the *CO intermediate, have been heralded as the most effective catalysts for facilitating the conversion of CO_2 into valuable hydrocarbons.[10,11] In pursuit of this, a spectrum of Cu-based electrocatalysts, encompassing metallic Cu, Cu oxides,[12–14] Cu-integrated metal–organic frameworks (MOFs),[15,16] and Cu-centric molecules,[17,18] have been meticulously developed, marking significant strides in the electrocatalytic conversion of CO_2 to CH$_4$ or C$_2$H$_4$. Nevertheless, the design of cost-effective and durable catalysts tailored for the targeted transformation of CO_2 into high-energy products continues to pose a formidable challenge.

The mechanism underlying the CO$_2$RR involves the initial reduction of CO_2 to adsorbed *CO, succeeded by *CO hydrogenation and/or C–C coupling processes.[8,19] Recent investigations have illuminated that *CO hydrogenation to *CHO represents the rate-limiting step in CH$_4$ generation, while *CHO also acts as a pivotal intermediate for multi-carbon (C$_2$) products.[4,20] Moreover, the journey from *CO to hydrocarbons encapsulates a multi-step hydrogenation sequence, with *H emerging as a crucial intermediary for hydrocarbon synthesis.

Consequently, fine-tuning the adsorption dynamics of *CO and *H presents a promising avenue for steering the CO_2RR towards desired products, particularly for CH_4 and C_2H_4. For example, Zheng et al. showcased that the strategic incorporation of two metal dopants, Zn and Mn, into Cu matrices could simultaneously modulate the coverage of *H and *CO, enabling the fine-tuning of selectivity between CH_4 and C_2H_4.[21] Similarly, Sargent et al. effectively manipulated *CO coverage through varying CO_2 concentrations, achieving tunable product specificity from C_2H_4 to CH_4.[22] In a parallel vein, Wei and colleagues enhanced the adsorption of the CO intermediate by augmenting polyaniline on Cu substrates, thereby activating CO_2 molecules and yielding a significant faradaic efficiency (FE) for C_2 products.[23] Despite these advances, attaining high selectivity shifts between desired products using analogous materials remains elusive, thereby underscoring the impetus for novel catalyst development.

In this report, we introduce an innovative strategy employing functional rare-earth metal oxides to facilitate selectivity switching between CH_4 and C_2H_4 products by modulating *H and *CO adsorption (Fig. 1). Two distinct electrocatalysts, Cu/CeO_x and a Cu/$CuCeO_x$ solid solution ($0 < X < 2$), were synthesized, with the CeO_x component enhancing *H coverage through expedited water dissociation, while $Cu–Ce–O_x$ solid solutions stabilize Cu^+ species, augmenting *CO adsorption and catalyzing the C–C coupling process. Electrochemical CO_2RR evaluations revealed that the Cu/$CuCeO_x$ catalyst achieved an ethylene FE of 40.2% at a partial current density of -245.7 mA cm^{-2}, in contrast to the Cu/CeO_x variant, which exhibited a methane FE of 38.6% at a partial current density of -198.3 mA cm^{-2}. Density functional theory (DFT) calculations further illustrated that $Cu–Ce–O_x$ solid solutions significantly reduce the formation energy of the *COCHO intermediate, thereby enhancing C_2H_4 production. This paradigm of adjusting CO_2RR selectivity via intermediary coverage heralds new avenues for designing innovative Cu-based nanocomposite catalysts.

Results and discussion

The Cu/$CuCeO_x$ catalyst was synthesized utilizing the co-precipitation methodology delineated in previous studies,[24] and subsequently subjected to annealing in a mixed atmosphere of 5 vol% H_2/Ar (Fig. 2a and S1†). In contrast, the Cu/CeO_x catalyst was fabricated through a bifurcated procedure: initially, CeO_x was prepared devoid of any Cu precursor via
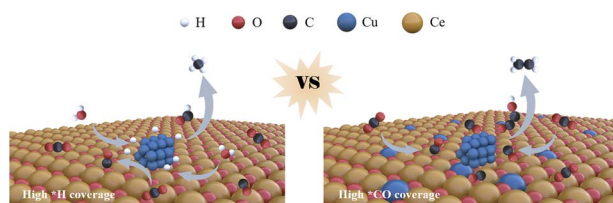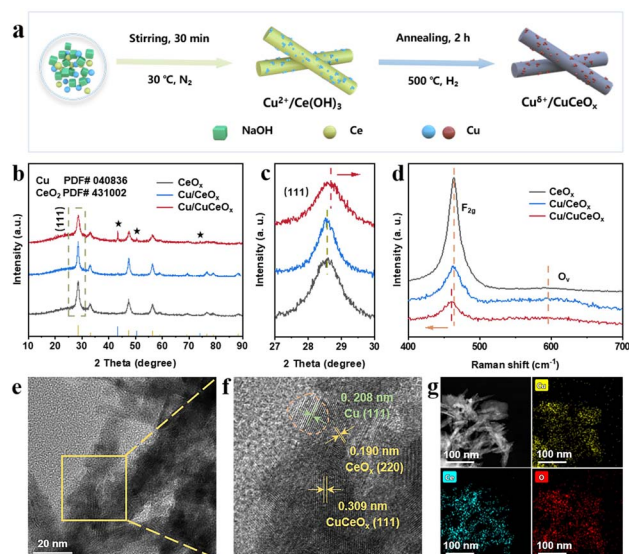

Fig. 2 (a) Synthetic route of the Cu/$CuCeO_x$ catalyst by a coprecipitation method. (b) XRD spectra, (c) local amplification of (111) and (d) Raman spectra for CeO_x, Cu/CeO_x, and Cu/$CuCeO_x$ catalysts (CeO_2, yellow, PDF# 43-1002; Cu, blue, PDF# 04-0836). (e and f) HRTEM images and (g) EDX elemental distribution mapping images of Cu/$CuCeO_x$.

coprecipitation; thereafter, Cu/CeO_x was produced by an impregnation technique. The X-ray diffraction (XRD) analysis of the synthesized samples (Fig. 2b) reveals diffraction peaks at 28.55°, 32.08°, 47.48°, 56.34°, 59.09°, 69.42°, 76.70°, 79.08°, and 88.43°, congruent with the established cubic fluorite-like structure of CeO_2 (PDF# 43-1002). Additionally, characteristic diffraction peaks of Cu are discernible (indicated by a pentagram at 43.30°, 50.43°, and 74.13°) corresponding to PDF# 04-0836. Notably, the (111) plane of Cu/$CuCeO_x$ exhibits a discernible shift towards higher Bragg angles compared to CeO_x and Cu/CeO_x (Fig. 2c), suggesting the formation of a Cu–Ce–O_x solid solution due to the substitution of a larger cation by a smaller one.[25–27] As the Cu content continues to increase, some of the copper precipitates out, forming clustered copper species on the Cu/$CuCeO_x$ nanorods.[28] And no diffraction peaks corresponding to Cu can be found when the copper loading is below 30 wt%, which may be due to the high dispersion of Cu nanoparticles with too small particle sizes on the surface of the ceria support to be identified by the XRD (Fig. S2†).[29,30] Raman spectroscopy of the catalysts reveals an intense band around 459 cm^{-1} and another at approximately 595 cm^{-1}, corresponding to the F_{2g} vibration pattern and defect-induced mode (O_v) in a cubic fluorite structure, respectively.[31] Notably, the F_{2g} bands of Cu/$CuCeO_x$ exhibit a redshift to lower frequencies with increasing Cu loading, compared to pure CeO_x (Fig. S3†), indicative of Cu atom doping into the CeO_x lattice and Cu/$CuCeO_x$ interface formation.[32,33] This results in extended Ce–O bond lengths at the interface and lattice distortions due to the atomic radius disparity between Cu^+ and Ce^{4+}/Ce^{3+},[34,35] corroborating the XRD findings.

Transmission electron microscopy (TEM, Fig. S4†) images depict the Cu/$CuCeO_x$ as possessing rod-like nanostructures.

Fig. 1 Diagrams of methane and ethylene production on Cu/CeO_x and Cu/$CuCeO_x$ during the CO_2RR, respectively.

20116 | J. Mater. Chem. A, 2024, 12, 20115–20120

This journal is © The Royal Society of Chemistry 2024

The dynamic light scattering in Fig. S5† further illustrates that the particle size distribution between 50 and 200 nm is slightly wider than that presented by TEM, which may be caused by partial rupture or aggregation of cerium dioxide. High-resolution TEM (HRTEM) images (Fig. 2e and f) identify the main interplanar spacings of 0.309 nm corresponding to the Cu–Ce–O$_x$ (111), slightly smaller than the Cu/CeO$_x$'s CeO$_2$ (111) plane (0.312 nm) observed in Fig. S6.† Other characteristic d-spacings at 0.190 and 0.208 nm correspond to the CeO$_2$ (220) and Cu (111) planes, respectively. Elemental mapping *via* energy-dispersive X-ray spectroscopy (EDS, Fig. 2g) confirms the uniform distribution of Cu, Ce, and O within Cu/CuCeO$_x$ without significant agglomeration. Moreover, inductively coupled plasma atomic emission spectroscopy (ICP-OES) quantified the Ce and Cu composition, aligning closely with theoretical expectations (Table S1†).

The valence states and surface chemistry of Cu, Ce, and O were investigated by X-ray photoelectron spectroscopy (XPS). The Ce 3d XPS spectra for both Cu/CeO$_x$ and Cu/CuCeO$_x$ nanorods, depicted in Fig. 3a, were deconvoluted into eight peaks corresponding to Ce 3d$_{5/2}$ (v, 882.4 eV; v′,884.9 eV; v″, 888.7 eV; v‴, 898.2 eV) and Ce 3d$_{3/2}$ states (μ, 900.8 eV; μ′, 903.5 eV; μ″, 907.2 eV; μ‴, 916.6 eV).[36,37] Peaks designated v, v″, v‴, μ, μ″, and μ‴ are indicative of Ce^{4+} species, while the v′ and μ′ peaks are attributed to Ce^{3+} species, denoting the coexistence of Ce^{4+} and Ce^{3+} within the composite matrix.[38] The relative abundance of Ce^{3+} to total cerium species was quantitatively assessed and was summarized in Table S1.† The ratio of Ce^{3+} in Cu/CeO$_x$ and Cu/CuCeO$_x$ is 0.114 and 0.128, respectively. A noteworthy observation was the positive shift in the Ce^{4+} peaks for Cu/CuCeO$_x$ (Fig. S7†), suggestive of alterations in the central charge distribution between Cu and Ce.[39] The Cu/CuCeO$_x$ exhibited a predominance of Ce^{3+} species, which are postulated to facilitate rapid electron transport and mitigate electron localization at the Cu^{2+}/Cu$^+$ sites within the Cu–Ce–O$_x$ solid solution matrix.[40] The O 1s XPS spectra are analyzed in Fig. 3b,

which can be resolved into two distinct peaks by deconvolution: one at a lower binding energy of 529.3 eV associated with lattice oxygen (O$_{latt}$) and another at 531.3 eV, ascribed to adsorbed oxygen species (O$_{ads}$).[41] The number of oxygen vacancies calculated from the deconvoluted core level O 1s spectra is shown in Table S1.† The Cu 2p XPS spectra (Fig. 3c) exhibit binding energies of 952.7 eV and 932.9 eV, characteristic of Cu$^+$ or Cu^0 species.[42,43] A minor presence of CuO, attributed to inevitable surface oxidation, was also noted.[39,44] Given the challenges in distinguishing between Cu^0 and Cu$^+$ based on Cu 2p$_{3/2}$ spectra alone,[29] additional analysis was conducted using Cu LMM Auger kinetic energy spectra (Fig. 3d), where peaks at 570.0 and 565.3 eV substantiate the presence of Cu$^+$ and Cu^0 species, respectively.[45,46] Herein, most of the Cu on the surface is oxidized to monovalent Cu species. The Cu/CuCeO$_x$ sample possesses the most surface monovalent Cu species (0.78), much higher than that of Cu/CeO$_x$ (0.56). The presence of monovalent copper is conducive to the adsorption of *CO.[47]

The CO$_2$RR catalytic performances of Cu/CuCeO$_x$ catalysts were tested in a flow cell, in which 1.0 M KOH was used as the electrolyte. In this work, all the applied potentials were converted into a reversible hydrogen electrode (RHE) scale without *iR* correction. The linear sweep voltammetry curves (LSV) shown in Fig. 4a were recorded by feeding the CO$_2$ gas across the 1.0 M KOH interface. Note that the Cu/CuCeO$_x$ catalysts exhibited higher current density responses than those of CeO$_x$ and Cu/CeO$_x$ catalysts, and we assume that the formation of Cu–Ce–O$_x$ solid solutions may enrich active sites that kinetically favored the CO$_2$RR. To verify the hypothesis, we conducted the cyclic voltammetry (CV) method to estimate the electrochemically active surface area (ECSA) of the catalysts (Fig. S8†). The results show that Cu/CuCeO$_x$ had larger ECSA values than the Cu/CeO$_x$ catalyst, indicating that the generation of Cu–Ce–O$_x$ solid
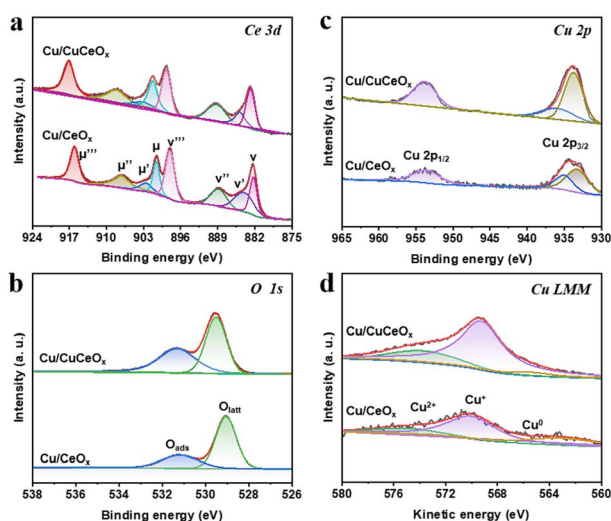

Fig. 3 XPS analysis of (a) Ce 3d, (b) O 1s, (c) Cu 2p, and (d) Cu LMM Auger spectra for Cu/CeO$_x$ and Cu/CuCeO$_x$.
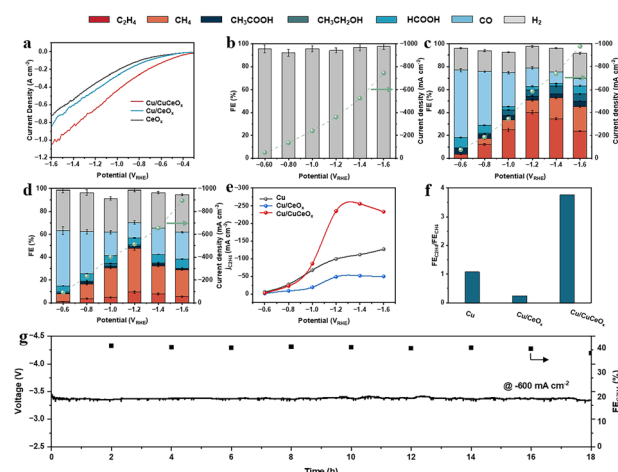

Fig. 4 (a) LSV spectra of CeO$_x$, Cu/CeO$_x$, and Cu/CuCeO$_x$ catalysts. (b–d) FEs of products at different applied potentials in 1.0 M KOH electrolyte for CeO$_x$, Cu/CuCeO$_x$, and Cu/CeO$_x$. (e) C$_2$H$_4$ partial current densities of Cu, Cu/CeO$_x$ and Cu/CuCeO$_x$ under different potentials. (f) FE$_{C_2H_4}$/FE$_{CH_4}$ of CeO$_x$, Cu/CeO$_x$, and Cu/CuCeO$_x$ at −1.2 V$_{RHE}$. (g) Stability test of Cu/CuCeO$_x$ during 18 h of long-time operation at −600 mA cm^{-2}.

This journal is © The Royal Society of Chemistry 2024

J. Mater. Chem. A, 2024, **12**, 20115–20120 | **20117**

solutions favors the kinetics of the CO_2RR *via* generating more interfacial active sites, which is consistent with the results of impedance analysis (Fig. S9†).

The gaseous and liquid products were quantitatively analyzed by on-line gas chromatography (GC, Fig. S10†) and ^1H nuclear magnetic resonance (^1H NMR, Fig. S11†), respectively.[48] For the pure CeO_2 catalyst, H_2 was the main product (Fig. 4b). As shown in Fig. 4c, the $Cu/CuCeO_x$ catalyst exhibited a high $FE_{C_2H_4}$ of 40.2% at -1.2 V_{RHE}. In comparison, the Cu and Cu/CeO_x catalysts showed lower $FE_{C_2H_4}$ at -1.2 V_{RHE} (Fig. 4d and S12†). For the pure Cu catalyst, the major products were H_2, CH_4, and C_2H_4 species, while FE_{CH_4} and $FE_{C_2H_4}$ were 18.9% and 20.5%, respectively (Fig. S12†). In contrast, for the Cu/CeO_x catalyst, CH_4 emerged as the predominant product, achieving a FE of 38.6% at a potential of -1.2 V_{RHE}. The comparison of FE for H_2 and the CH_4 products over those three catalysts further demonstrated that the formation of H_2 and the CH_4 species was suppressed on the $Cu/CuCeO_x$ catalyst. Furthermore, LSV measurements in an Ar-saturated 1.0 M KOH electrolyte without CO_2 gas revealed that CeO_x exhibited the lowest overpotential at equivalent current densities, further affirming its proficiency in hydrogen evolution (Fig. S13†). Furthermore, the $Cu/CuCeO_x$ catalyst demonstrated the highest partial current density for C_2H_4 production (Fig. 4e), signifying that $Cu/CuCeO_x$ has superior catalytic activity for C_2H_4 synthesis compared to both pristine Cu and Cu/CeO_x. Fig. 4f illustrates that the $FE_{C_2H_4}/FE_{CH_4}$ ratio achieved a maximum of 3.77 on $Cu/CuCeO_x$, compared to 1.08 and 0.25 for Cu and Cu/CeO_x, respectively, indicating that the formation of $Cu–Ce–O_x$ solid solutions is particularly conducive to C_2H_4 production. Comparative electrochemical evaluations of $Cu_{0.1}/CuCeO_x$ and $Cu_{0.5}/CuCeO_x$, synthesized *via* the same method, were also performed (Fig. S14†). A 50% increase in Cu loading led to a decline in C_2H_4 selectivity, potentially due to the formation of larger Cu particles, which diminish the number of Cu active sites directly interacting with Ce, thereby inhibiting C–C coupling.[36] The long-term stability of $Cu/CuCeO_x$ was assessed through chronopotentiometry, and no significant decrease in Faraday efficiency of C_2H_4 was observed during 18 h of electrocatalysis at -600 mA cm^{-2} (Fig. 4g). Post-CO_2RR XPS analysis of the electrode confirmed the persistence of Cu^+ as the predominant valence state in $Cu/CuCeO_x$, indirectly evidencing the stabilizing influence of the $Cu–Ce–O_x$ matrix on Cu^+ species (Fig. S15 and Table S1†). The efficient presence of Cu^+ was also demonstrated by *in situ* Raman spectra of a wide potential window (Fig. S16†), with characteristic peaks around 150, 230 and 500 cm^{-1}.[49,50] Moreover, the characteristic peaks of the *CO (2050 cm^{-1}) intermediates were also observed, further indicating the high *CO concentration on the $Cu/CuCeO_x$ catalyst surface.

Subsequent density functional theory (DFT) calculations were conducted for Cu/CeO_x and $Cu/CuCeO_x$ catalysts to rationalize the effects of $Cu–Ce–O_x$ solid solutions on the CO_2RR selectivity toward C_2H_4 (Experimental section in the ESI, Fig. S17 and S18†). Initially, Bader charge analysis was applied to $Cu/CuCeO_x$ (Fig. 5a), revealing that copper integration into the cerium dioxide matrix diminished the charge density around the Cu sites, indicating that the charges of Cu and Ce were
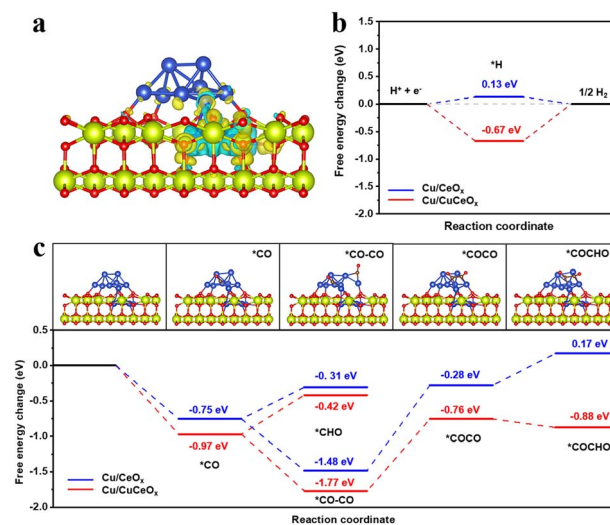

Fig. 5 (a) The Bader charge of $Cu/CuCeO_x$. (b) Desorption energy diagram of hydrogen on Cu/CeO_x and $Cu/CuCeO_x$. (c) The free energy change diagram of *CHO or *COCHO generated by *CO over the Cu/CeO_x and $Cu/CuCeO_x$.

rearranged.[51] The transfer of electrons from Cu to Ce^{3+} results in higher Cu^+ in $Cu/CuCeO_x$, which is conducive to promoting the adsorption of *CO on the surface and enhancing C–C to achieve high selectivity of C_2H_4. This alteration favorably impacts the protonation of *COCO intermediates, thereby facilitating C_2H_4 formation. In addition, the hydrogen evolution reaction (HER) performance of both Cu/CeO_x and $Cu/CeCuO_x$ was assessed (Fig. 5b). The Gibbs free energy ($|\Delta G_{H*}|$) for the HER on Cu/CeO_x is 0.13 eV lower than that of $Cu/CeCuO_x$ (0.67 eV), thus allowing the promotion of the surface *H coverage and the hydrogenation.

The free energy diagrams depicting the formation of *CHO or *COCHO from *CO on the Cu/CeO_x or $Cu/CuCeO_x$ catalysts are presented in Fig. 5c. Moreover, $Cu/CuCeO_x$ also exhibits significantly stronger *CO adsorption than Cu/CuO_x, enhancing the local *CO concentration and favoring the C–C coupling process on the $Cu/CeCuO_x$ catalyst. According to previous reports,[52] the formation of CH_4 and C_2H_4 is primarily governed by distinct rate-determining steps: the hydrogenation of *CO to *CHO for CH_4, and the coupling of *CO with *CHO for C_2H_4, respectively.[20,53] For the Cu/CeO_x catalyst, the ΔG value of the CO hydrogenation is 0.44 eV lower than that of the $Cu/CeCuO_x$ catalyst, suggesting that Cu/CeO_x has a higher selectivity for producing CH_4. In contrast, the formation of the *COCHO intermediate of the $Cu/CuCeO_x$ catalyst (0.12 eV) requires less free energy change than that of the Cu/CuO_x catalyst (0.45 eV), indicating a more favorable C_2H_4 pathway. Our computational findings corroborated that surfaces characterized by relatively high *H and low *CO coverage are conducive to the promotion of CH_4 production. Conversely, surfaces with a rich presence of *CO and moderate levels of *H are advantageous for the synthesis of C_2H_4.

Lastly, *in situ* infrared spectroscopy was employed to analyze potential surface intermediates on Cu/CeO_x and $Cu/CuCeO_x$

20118 | *J. Mater. Chem. A*, 2024, **12**, 20115–20120

This journal is © The Royal Society of Chemistry 2024

under various potential conditions, further elucidating the catalytic mechanism (Fig. S19†). Not only the peak of CO_2 can be observed in a pronounced absorption band of 2400–2300 cm^{-1},[54,55] but also the characteristic peak of CO (2050 cm^{-1}) can also be identified,[56] which serves as evidence for the activation and reduction of CO_2.[57] In addition, a distinct *CHO peak, key intermediate for CH_4, was further found at 1226 cm^{-1}.[58] In contrast, in the $Cu/CuCeO_x$ spectrum, the characteristic peak of *CHO is significantly weakened and replaced by *COCHO at 1550 and 1185 cm^{-1},[59–62] indicating that $Cu/CuCeO_x$ catalysts are more inclined to produce C_2, which is consistent with the results calculated by DFT.

Conclusions

In summary, this study successfully demonstrates the selective electroreduction of CO_2 to CH_4 or C_2H_4 by finely tuning *H and *CO adsorption on Cu/CeO_x catalysts. Our innovative approach, involving the manipulation of Cu/CeO_x and $Cu/CuCeO_x$ interfaces, significantly influences the catalytic selectivity towards desired C_1 or C_2 products. Notably, the $Cu/CuCeO_x$ electrocatalyst demonstrated a peak $FE_{C_2H_4}$ of 40.2% and $j_{C_2H_4}$ of −245.7 mA cm^{-2}, while the Cu/CeO_x electrocatalyst showed good CO_2RR performances with a maximum FE_{CH_4} of 38.6% and j_{CH_4} of −198.3 mA cm^{-2}. This advancement is underpinned by the enhanced *CO adsorption facilitated by the stabilization of Cu^+ species within the $Cu–Ce–O_x$ solid solution. Our findings pave the way for the development of tailored catalysts capable of directing CO_2 electroreduction towards specific hydrocarbons, addressing critical needs in CO_2 mitigation and sustainable fuel production.

Data availability

All the data supporting this article have been included in the main text and the ESI.†

Author contributions

M. K. proposed, designed, and supervised the project. T. H., Y. B., Z. C., and J. P. wrote the manuscript. T. H., Y. B., and Z. C. performed the experiments and analyzed the data. All authors discussed the results and revised the manuscript.

Conflicts of interest

The authors declare no conflicts of interest.

Acknowledgements

References

1 M. Li, F. Zhang, M. Kuang, Y. Ma, T. Liao, Z. Sun, W. Luo, W. Jiang and J. Yang, *Nano-Micro Lett.*, 2023, **15**, 238.

2 M. B. Ross, P. De Luna, Y. Li, C.-T. Dinh, D. Kim, P. Yang and E. H. Sargent, *Nat. Catal.*, 2019, **2**, 648.

3 Y. Ma, J. Wang, J. Yu, J. Zhou, X. Zhou, H. Li, Z. He, H. Long, Y. Wang, P. Lu, J. Yin, H. Sun, Z. Zhang and Z. Fan, *Matter*, 2021, **4**, 888.

4 W. Ma, S. Xie, T. Liu, Q. Fan, J. Ye, F. Sun, Z. Jiang, Q. Zhang, J. Cheng and Y. Wang, *Nat. Catal.*, 2020, **3**, 478.

5 H. Chen, Z. Wang, X. Wei, S. Liu, P. Guo, P. Han, H. Wang, J. Zhang, X. Lu and B. Wei, *Appl. Surf. Sci.*, 2021, **544**, 148965.

6 W. Ma, S. Xie, X.-G. Zhang, F. Sun, J. Kang, Z. Jiang, Q. Zhang, D.-Y. Wu and Y. Wang, *Nat. Commun.*, 2019, **10**, 892.

7 W. Zhu, L. Fan, Q. Geng, C. Wang, X. Fan, Y. Zhang and C. Li, *Chem. Eng. J.*, 2024, **489**, 151316.

8 S. Jin, Z. Hao, K. Zhang, Z. Yan and J. Chen, *Angew. Chem., Int. Ed.*, 2021, **60**, 20627–20648.

9 Q.-J. Wu, D.-H. Si, P.-P. Sun, Y.-L. Dong, S. Zheng, Q. Chen, S.-H. Ye, D. Sun, R. Cao and Y.-B. Huang, *Angew. Chem., Int. Ed.*, 2023, **62**, e202306822.

10 J. Zhang, C. Guo, S. Fang, X. Zhao, L. Li, H. Jiang, Z. Liu, Z. Fan, W. Xu, J. Xiao and M. Zhong, *Nat. Commun.*, 2023, **14**, 1298.

11 Z. Zhang, L. Bian, H. Tian, Y. Liu, Y. Bando, Y. Yamauchi and Z.-L. Wang, *Small*, 2022, **18**, 2107450.

12 H. Shi, L. Luo, C. Li, Y. Li, T. Zhang, Z. Liu, J. Cui, L. Gu, L. Zhang, Y. Hu, H. Li and C. Li, *Adv. Funct. Mater.*, 2024, **34**, 2310913.

13 Y. Sun, J. Xie, Z. Fu, H. Zhang, Y. Yao, Y. Zhou, X. Wang, S. Wang, X. Gao, Z. Tang, S. Li, X. Wang, K. Nie, Z. Yang and Y.-M. Yan, *ACS Nano*, 2023, **17**, 13974.

14 L. Ma, Q. Geng, L. Fan, J.-X. Li, D. Du, J. Bai and C. Li, *Nano Res.*, 2023, **16**, 9065–9072.

15 X. Xie, X. Zhang, M. Xie, L. Xiong, H. Sun, Y. Lu, Q. Mu, M. H. Rummeli, J. Xu, S. Li, J. Zhong, Z. Deng, B. Ma, T. Cheng, W. A. Goddard and Y. Peng, *Nat. Commun.*, 2022, **13**, 63.

16 T. Yan, P. Wang and W.-Y. Sun, *Small*, 2023, **19**, 2206070.

17 Q. Bie, H. Yin, Y. Wang, H. Su, Y. Peng and J. Li, *Chin. J. Catal.*, 2024, **57**, 96.

18 T. Zheng, C. Liu, C. Guo, M. Zhang, X. Li, Q. Jiang, W. Xue, H. Li, A. Li, C.-W. Pao, J. Xiao, C. Xia and J. Zeng, *Nat. Nanotechnol.*, 2021, **16**, 1386.

19 C. Chen, S. Yu, Y. Yang, S. Louisia, I. Roh, J. Jin, S. Chen, P.-C. Chen, Y. Shan and P. Yang, *Nat. Catal.*, 2022, **5**, 878.

20 J. Feng, L. Zhang, S. Liu, L. Xu, X. Ma, X. Tan, L. Wu, Q. Qian, T. Wu, J. Zhang, X. Sun and B. Han, *Nat. Commun.*, 2023, **14**, 4615.

21 Y. Chen, N. Lyu, J. Zhang, S. Yan, C. Peng, C. Yang, X. Lv, C. Hu, M. Kuang and G. Zheng, *Small*, 2024, 2308004.

22 X. Wang, A. Xu, F. Li, S.-F. Hung, D.-H. Nam, C. M. Gabardo, Z. Wang, Y. Xu, A. Ozden, A. S. Rasouli, A. H. Ip, D. Sinton and E. H. Sargent, *J. Am. Chem. Soc.*, 2020, **142**, 3525.

23 Q. Zhao, J. M. P. Martirez and E. A. Carter, *J. Am. Chem. Soc.*, 2021, **143**, 6152.

This journal is © The Royal Society of Chemistry 2024

J. Mater. Chem. A, 2024, **12**, 20115–20120 | **20119**

24 X. Guo, W. Ye, Z. a. Chen, A. Zhou, D. Jin and T. Ma, *Appl. Catal., B*, 2022, **310**, 121334.

25 W. Shan, W. Shen and C. Li, *Chem. Mater.*, 2003, **15**, 4761.

26 W. Liu, X. Liu, L. Feng, J. Guo, A. Xie, S. Wang, J. Zhang and Y. Yang, *Nanoscale*, 2014, **6**, 10693.

27 C.-A. Thieu, S. Yang, H.-I. Ji, H. Kim, K. J. Yoon, J.-H. Lee and J.-W. Son, *J. Mater. Chem. A*, 2022, **10**, 2460.

28 J. Jiang, H. Yang, H. Jiang, Y. Hu and C. Li, *Chem. Eng. J.*, 2023, **471**, 144439.

29 C. He, Y. Yu, L. Yue, N. Qiao, J. Li, Q. Shen, W. Yu, J. Chen and Z. Hao, *Appl. Catal., B*, 2014, **147**, 156.

30 P. Bera, K. R. Priolkar, P. R. Sarode, M. S. Hegde, S. Emura, R. Kumashiro and N. P. Lalla, *Chem. Mater.*, 2002, **14**, 3591.

31 B. Levasseur, A. M. Ebrahim and T. J. Bandosz, *Langmuir*, 2011, **27**, 9379.

32 T. Masui, K. Koyabu, K. Minami, T. Egawa and N. Imanaka, *J. Phys. Chem. C*, 2007, **111**, 13892.

33 S. Zhang, B. Jiang, M. Tong, Y. Yang, Z. Liao, Z. Huang, J. Sun, J. Wang and Y. Yang, *Ind. Eng. Chem. Res.*, 2023, **62**, 20667.

34 F. Jiang, S. Wang, B. Liu, J. Liu, L. Wang, Y. Xiao, Y. Xu and X. Liu, *ACS Catal.*, 2020, **10**, 11493.

35 H. Sun, H. Wang and Z. Qu, *ACS Catal.*, 2023, **13**, 1077.

36 S. Jin, D. Li, Z. Wang, Y. Wang, L. Sun and M. Zhu, *Catal. Sci. Technol.*, 2022, **12**, 7003.

37 M. Yusufoğlu, S. Tafazoli, H. Jahangiri, M. B. Yağcı, T. Balkan and S. Kaya, *ACS Appl. Mater. Interfaces*, 2024, **16**, 7288.

38 C. W. Lee, S.-J. Shin, H. Jung, D. L. T. Nguyen, S. Y. Lee, W. H. Lee, D. H. Won, M. G. Kim, H.-S. Oh, T. Jang, H. Kim, B. K. Min and Y. J. Hwang, *ACS Energy Lett.*, 2019, **4**, 2241.

39 G. Tang, Y. Wu, J. Zhao, H. Zhang, M. Zhou and Y. Wang, *Chem.–Eur. J.*, 2022, **28**, e202103459.

40 Z. Yang, D. Ji, Z. Li, Z. He, Y. Hu, J. Yin, Y. Hou, P. Xi and C.-H. Yan, *Small*, 2023, **19**, 2303099.

41 W. Wang, Q. Zhu, F. Qin, Q. Dai and X. Wang, *Chem. Eng. J.*, 2018, **333**, 226.

42 R. Feng, Q. Zhu, M. Chu, S. Jia, J. Zhai, H. Wu, P. Wu and B. Han, *Green Chem.*, 2020, **22**, 7560.

43 J. Shan, Y. Shi, H. Li, Z. Chen, c. Sun, Y. Shuai and Z. Wang, *Chem. Eng. J.*, 2022, **433**, 133769.

44 K. Cao, H. Liu, W. Li, Q. Han, Z. Zhang, K. Huang, Q. Jing and L. Jiao, *Small*, 2019, **15**, 1901775.

45 S. Y. Lee, H. Jung, N.-K. Kim, H.-S. Oh, B. K. Min and Y. J. Hwang, *J. Am. Chem. Soc.*, 2018, **140**, 8681.

46 N. Martić, C. Reller, C. Macauley, M. Löffler, B. Schmid, D. Reinisch, E. Volkova, A. Maltenberger, A. Rucki, K. J. J. Mayrhofer and G. Schmid, *Adv. Energy Mater.*, 2019, **9**, 1901228.

47 B. Yang, W. Deng, L. Guo and T. Ishihara, *Chin. J. Catal.*, 2020, **41**, 1348–1359.

48 S. Liu, Y. Cao, H. Liu, H. Wang, B. Zhang, Y. Zhang, L. Zhang, S. Zhang and J. Sun, *Nanoscale*, 2021, **13**, 16986.

49 A. Xu, S.-F. Hung, A. Cao, Z. Wang, N. Karmodak, J. E. Huang, Y. Yan, A. Sedighian Rasouli, A. Ozden, F.-Y. Wu, Z.-Y. Lin, H.-J. Tsai, T.-J. Lee, F. Li, M. Luo, Y. Wang, X. Wang, J. Abed, Z. Wang, D.-H. Nam, Y. C. Li, A. H. Ip, D. Sinton, C. Dong and E. H. Sargent, *Nat. Catal.*, 2022, **5**, 1081–1088.

50 M. Wang, Z. Wang, Z. Huang, M. Fang, Y. Zhu and L. Jiang, *ACS Nano*, 2024, **18**, 15303–15311.

51 J. Zhang, P. Yu, C. Peng, X. Lv, Z. Liu, T. Cheng and G. Zheng, *ACS Catal.*, 2023, **13**, 7170.

52 L. Xiong, X. Zhang, L. Chen, Z. Deng, S. Han, Y. Chen, J. Zhong, H. Sun, Y. Lian, B. Yang, X. Yuan, H. Yu, Y. Liu, X. Yang, J. Guo, M. H. Rümmeli, Y. Jiao and Y. Peng, *Adv. Mater.*, 2021, **33**, 2101741.

53 A. Vasileff, C. Xu, Y. Jiao, Y. Zheng and S. Z. Qiao, *Chem*, 2018, **4**, 1809.

54 G. N. Vayssilov, M. Mihaylov, P. S. Petkov, K. I. Hadjiivanov and K. M. Neyman, *J. Phys. Chem. C*, 2011, **115**, 23435.

55 Y. Yan, R. J. Wong, Z. Ma, F. Donat, S. Xi, S. Saqline, Q. Fan, Y. Du, A. Borgna, Q. He, C. R. Müller, W. Chen, A. A. Lapkin and W. Liu, *Appl. Catal., B*, 2022, **306**, 121098.

56 J. Yin, Z. Gao, F. Wei, C. Liu, J. Gong, J. Li, W. Li, L. Xiao, G. Wang, J. Lu and L. Zhuang, *ACS Catal.*, 2022, **12**, 1004.

57 Y. Katayama, F. Nattino, L. Giordano, J. Hwang, R. R. Rao, O. Andreussi, N. Marzari and Y. Shao-Horn, *J. Phys. Chem. C*, 2019, **123**, 5951.

58 P. Wang, H. Yang, C. Tang, Y. Wu, Y. Zheng, T. Cheng, K. Davey, X. Huang and S.-Z. Qiao, *Nat. Commun.*, 2022, **13**, 3754.

59 L. Zhang, J. Feng, L. Wu, X. Ma, X. Song, S. Jia, X. Tan, X. Jin, Q. Zhu, X. Kang, J. Ma, Q. Qian, L. Zheng, X. Sun and B. Han, *J. Am. Chem. Soc.*, 2023, **145**, 21945.

60 Q. Geng, L. Fan, H. Chen, C. Zhang, Z. Xu, Y. Tian, C. Yu, L. Kang, Y. Yamauchi, C. Li and L. Jiang, *J. Am. Chem. Soc.*, 2024, **146**, 10599–10607.

61 L. Fan, Q. Geng, L. Ma, C. Wang, J.-X. Li, W. Zhu, R. Shao, W. Li, X. Feng, Y. Yamauchi, C. Li and L. Jiang, *Chem. Sci.*, 2023, **14**, 13851–13859.

62 S. Hu, Y. Chen, Z. Zhang, S. Li, H. Liu, X. Kang, J. Liu, S. Ge, J. Wang, W. Lv, Z. Zeng, X. Zou, Q. Yu and B. Liu, *Small*, 2024, **20**, 2308226.

20120 | *J. Mater. Chem. A*, 2024, **12**, 20115–20120

This journal is © The Royal Society of Chemistry 2024